Available online at www.sciencedirect.com

ScienceDirect

Geochimica et Cosmochimica Acta 146 (2014) 59–75

Geochimica et Cosmochimica Acta

www.elsevier.com/locate/gca

Copper and iron isotope fractionation during weathering and pedogenesis: Insights from saprolite profiles

Sheng-Ao Liu [a,*], Fang-Zhen Teng [b], Shuguang Li [a,c], Gang-Jian Wei [d], Jing-Long Ma [d], Dandan Li [a]

[a] State Key Laboratory of Geological Processes and Mineral Resources, China University of Geosciences, Beijing 100083, China
[b] Isotope Laboratory, Department of Earth and Space Sciences, University of Washington, Seattle, WA 98195, USA
[c] CAS Key Laboratory of Crust-Mantle Materials and Environments, School of Earth and Space Sciences, University of Science and Technology of China, Hefei 230026, China
[d] Key Laboratory of Isotope Geochronology and Geochemistry, Guangzhou Institute of Geochemistry, Chinese Academy of Sciences, Guangzhou 510640, China

Received 20 November 2013; accepted in revised form 28 September 2014; available online 5 October 2014

Abstract

Iron and copper isotopes are useful tools to track redox transformation and biogeochemical cycling in natural environment. To study the relationships of stable Fe and Cu isotopic variations with redox regime and biological processes during weathering and pedogenesis, we carried out Fe and Cu isotope analyses for two sets of basalt weathering profiles (South Carolina, USA and Hainan Island, China), which formed under different climatic conditions (subtropical vs. tropical). Unaltered parent rocks from both profiles have uniform δ^{56}Fe and δ^{65}Cu values close to the average of global basalts. In the South Carolina profile, δ^{56}Fe values of saprolites vary from −0.01‰ to 0.92‰ in the lower (reduced) part and positively correlate with $Fe^{3+}/\Sigma Fe$ ($R^2 = 0.90$), whereas δ^{65}Cu values are almost constant. By contrast, δ^{56}Fe values are less variable and negatively correlate with $Fe^{3+}/\Sigma Fe$ ($R^2 = 0.88$) in the upper (oxidized) part, where large (4.85‰) δ^{65}Cu variation is observed with most samples enriched in heavy isotopes. In the Hainan profile formed by extreme weathering under oxidized condition, δ^{56}Fe values vary little (0.05–0.14‰), whereas δ^{65}Cu values successively decrease from 0.32‰ to −0.12‰ with depth below 3 m and increase from −0.17‰ to 0.02‰ with depth above 3 m. Throughout the whole profile, δ^{65}Cu positively correlate with Cu concentration and negatively correlate with the content of total organic carbon (TOC). Overall, the contrasting Fe isotopic patterns under different redox conditions suggest redox states play the key controls on Fe mobility and isotope fractionation. The negative correlation between δ^{56}Fe and $Fe^{3+}/\Sigma Fe$ in the oxidized part of the South Carolina profile may reflect addition of isotopically light Fe. This is demonstrated by leaching experiments, which show that Fe mineral pools extracted by 0.5 N HCl, representing poorly-crystalline Fe (hydr)-oxides, are enriched in light Fe isotopes. The systematic Cu isotopic variation in the Hainan profile reflects desorption and downward transport of isotopically heavy Cu, leaving the organically-bound Cu enriched in light isotope as supported by the negative correlation of δ^{65}Cu with TOC ($R^2 = 0.88$). The contrasting (mostly positive vs. negative) Cu isotopic signatures in the upper parts of these two profiles can be attributed to the different climatic conditions, e.g., high rainfall at a tropical climate in Hainan favors desorption and the development of organism, whereas relatively dry climate in South Carolina favors Cu re-precipitation from soil solutions and adsorption onto Fe (hydr)-oxides. Our results highlight the potential applications of Fe and Cu isotopes as great tracers of redox condition, ancient climate and biological cycling during chemical weathering and pedogenic translocation.

* Corresponding author at: The China University of Geosciences, No. 29, Xueyuan Road, Haidian District, Beijing 100083, China.
E-mail addresses: lsa@cugb.edu.cn, lsa@mail.ustc.edu.cn (S.-A. Liu).

http://dx.doi.org/10.1016/j.gca.2014.09.040
0016-7037/

1. INTRODUCTION

Continental weathering governs the production of soils from rocks and is an important process controlling the distribution of trace metals in natural systems (Liaghati et al., 2004). This process can impact the ecosystems by releasing dissolved metals and controlling their distribution in porewaters and contaminated soils (Rubio et al., 2000). Stable isotopic systematics of Fe and Cu may be excellent tools that could be used to trace biological cycles in soils (Anbar, 2004; Johnson et al., 2004; Dauphas and Rouxel, 2006; Bigalke et al., 2011). Towards a comprehensive understanding of the mechanism of Fe and Cu isotope fractionation during continental weathering, large amounts of data have been reported for dissolved Fe and Cu in rivers and seawaters (Bermin et al., 2006; Borrok et al., 2008; Vance et al., 2008; Kimball et al., 2009; Radic et al., 2011), for soils and associated porewaters (Fantle and DePaolo, 2004; Emmanuel et al., 2005; Thompson et al., 2007; Wiederhold et al., 2007; Poitrasson et al., 2008; Bigalke et al., 2010a, 2011; Mathur et al., 2012; Yesavage et al., 2012), as well as for experimental leaching of primary sulfide and silicate minerals (Brantley et al., 2004; Chapman et al., 2009; Fernandez and Borrok, 2009) and adsorption of Cu to mineral or bacteria surface (Balistrieri et al., 2008; Pokrovsky et al., 2008; Navarrete et al., 2011). These pioneering studies have documented that significant fractionations of both Fe and Cu isotopes can occur during mineral dissolution and adsorption involved in soil formation.

Soils are key components in the biological cycling of elements and represent the interface between the solid Earth, hydrosphere and biosphere at the Earth's surface. Studies of soil profiles can provide direct constraints on the behavior of metal isotopes during weathering and pedogenesis, in which various factors (e.g. redox condition, acidity, climate and biological effect etc.) may play different roles. Previous studies have suggested that there are multiple mechanisms fractionating Fe and Cu isotopes during continental weathering, including redox transformation (Fantle and DePaolo, 2004; Chapman et al., 2009; Mathur et al., 2012), precipitation, ad/desorption (Balistrieri et al., 2008), and biological processes (Mathur et al., 2005; Thompson et al., 2007; Wiederhold et al., 2007; Bigalke et al., 2010b; Kiczka et al., 2011; Yesavage et al., 2012). In most cases, however, isotopic variations observed in natural soils resulted from more than one process. Therefore it is difficult to unambiguously fingerprint the role of each process based on a single isotopic systematics.

Combined studies of Fe and Cu isotopic systematics have an important advantage in evaluating the roles of different mechanisms during continental weathering. This is because Fe and Cu behave differently in several ways although both are redox-sensitive. First, Fe(II) is generally more mobile and isotopically lighter than Fe(III) species whereas Cu(II) is more mobile and isotopically heavier than Cu(I) (Zhu et al., 2002; Fernandez and Borrok, 2009). The different mobility of Fe and Cu species can result in contrasting behaviors of Fe and Cu isotopes during mineral dissolution (Fernandez and Borrok, 2009). Thus, if only redox condition primarily controls element transformation and isotope fractionation, then opposite direction of Fe and Cu isotopic variations will be expected because higher valence state generally favors heavier isotopes. Second, Fe is a major constituent in most of silicate rocks primarily hosted by mafic minerals as well as in Fe-oxy-hydroxides, whereas Cu is a trace element and mainly hosted by easily-altered sulfide phases. This can result in different susceptibility of Fe and Cu transformation and isotope fractionation on the intensity of weathering (Mathur et al., 2012). Third, Cu can be strongly adsorbed onto clay minerals or Fe (hydr)-oxides (Dube et al., 2001), an additional process that may fractionate Cu isotopes relative to the dissolved or silicate-bound Cu (Balistrieri et al., 2008). Based on these potential differences, a combined study of Fe and Cu isotopes in the same soil samples can help demonstrate the role of different mechanisms in Fe or Cu isotope fractionation during continental weathering. To date, few studies have reported data for both Fe and Cu isotopes in the same soil samples.

In this study, we reported a combined study of Fe and Cu isotopes on two well-studied diabase and basalt weathering profiles from South Carolina, USA and Hainan Island, China, respectively (Gardner et al., 1981; Ma et al., 2007). Samples from these two profiles are suitable for this scientific subject because they are significantly different in the weathering intensity, oxidation conditions and climate conditions (subtropical vs. tropical). In addition, the Hainan profile displays significant variation in the amount of total organic carbon with depth, allowing the role of biological recycling on Cu or Fe isotope fractionation to be well evaluated. Finally, Mg isotopes have been analyzed for both profiles and Li isotopes have been studied for the South Carolina profile (Rudnick et al., 2004; Teng et al., 2010; Huang et al., 2012). Since both Mg and Li are redox-insensitive, comparisons of Fe and Cu isotopes with Mg and Li isotopes in the same profiles can further evaluate the role of redox conditions on Fe and Cu isotope fractionation, although these elements are probably controlled by different minerals. These two profiles thus provide natural examples documenting how Fe and Cu isotopes are fractionated during continental weathering associated with complicated variation of redox condition and formation of secondary minerals, as well as in the presence of organic matters.

2. SAMPLES

2.1. Diabase weathering profile from South Carolina, USA

The studied saprolite samples were collected along a nearly vertical profile from Cayce, South Carolina. The saprolites developed on Mesozoic diabases that cut a granite quarry as a dike (N33°58.09′, W81°03.07′) (Gardner et al., 1981). These saprolites formed during the Tertiary in a humid, subtropical climate, overlain by a thin (~2 m) layer of Coastal Plain sediment. The diabase dike is ~7 m wide, with saprolites developed within the top 11 m (Gardner et al., 1981). The unaltered diabase crops out below 11 m and contains plagioclase (40%), clinopyroxene (29%) and opaque minerals (3%) (Gardner et al., 1981).

In addition, it contains two unusual phases of talc (20%) and chlorite (8%). Green- and red-stained alteration haloes occur sequentially within the granite through that the dike cuts. These form a narrow (3–6 m thick) aureole in the upper part (0–6 m) of the profile, but increase in thickness up to ~30 m below 6 m depth.

Saprolite samples have been pulverized and analyzed for density, clay mineral proportions and bulk chemical compositions by Gardner et al. (1981). The weathering intensity gradationally increases with decreasing depth. The greatest amount of leaching occurred at the shallowest level due to rainwater infiltration as shown by the least density within the top 2 m. Kaolinite, smectite and Fe-oxides dominate secondary minerals in the saprolites.

The most striking feature of this weathering profile is a discontinuity that exists at ~2 m depth (Gardner et al., 1981). Both clay mineralogy and bulk chemistry show discontinuities and display different variation trends cross the discontinuity (Fig. 1). Bulk density generally increases with depth in the lower part (below 2 m) (Fig. 1b). Below 2 m, siderite veins were formed by weathering of original chlorite veins in the diabase. Towards the discontinuity, the ratio of kaolinite to smectite (K/S) increases reflecting transformation of smectite to kaolinite during progressing weathering, and bulk density decreases (Fig. 1a and b). Above 2 m, no siderite veins formed, the kaolinite/smectite ratio and bulk density are almost constant, and kaolinite and smectite contents decrease towards the surface (Gardner et al., 1981). Formation of the ~2 m discontinuity was interpreted by Gardner et al. (1981) as a result of an abrupt change in redox conditions. The upper part was oxidized, whereas the lower profile was reduced. There is also abrupt change of chemical compositions across the 2 m discontinuity (Fig. 1). Furthermore, below 2 m, chemical and lithium isotopic compositions show a discontinuity at 6 m depth, which has been interpreted to reflect the former presence of a water table at this depth (Gardner et al., 1981; Rudnick et al., 2004).

Sixteen saprolite samples from the weathering profile and one unaltered diabase at 30 m were analyzed for Fe and Cu isotopic compositions. The mineralogy, major and trace element geochemistry as well as Li and Mg isotopes for these samples were previously reported (Gardner et al., 1981; Rudnick et al., 2004; Teng et al., 2010).

2.2. Basalt weathering profile from Hainan Island, China

The weathering profile is exposed at a small hill in the northeastern region of the Hainan province in southern China. This region has a tropical, moist, monsoonal style climate, with a mean annual air temperature of 25 °C and mean annual precipitation of 1500 mm (Ma et al., 2007). Samples were collected with an uninterrupted progression

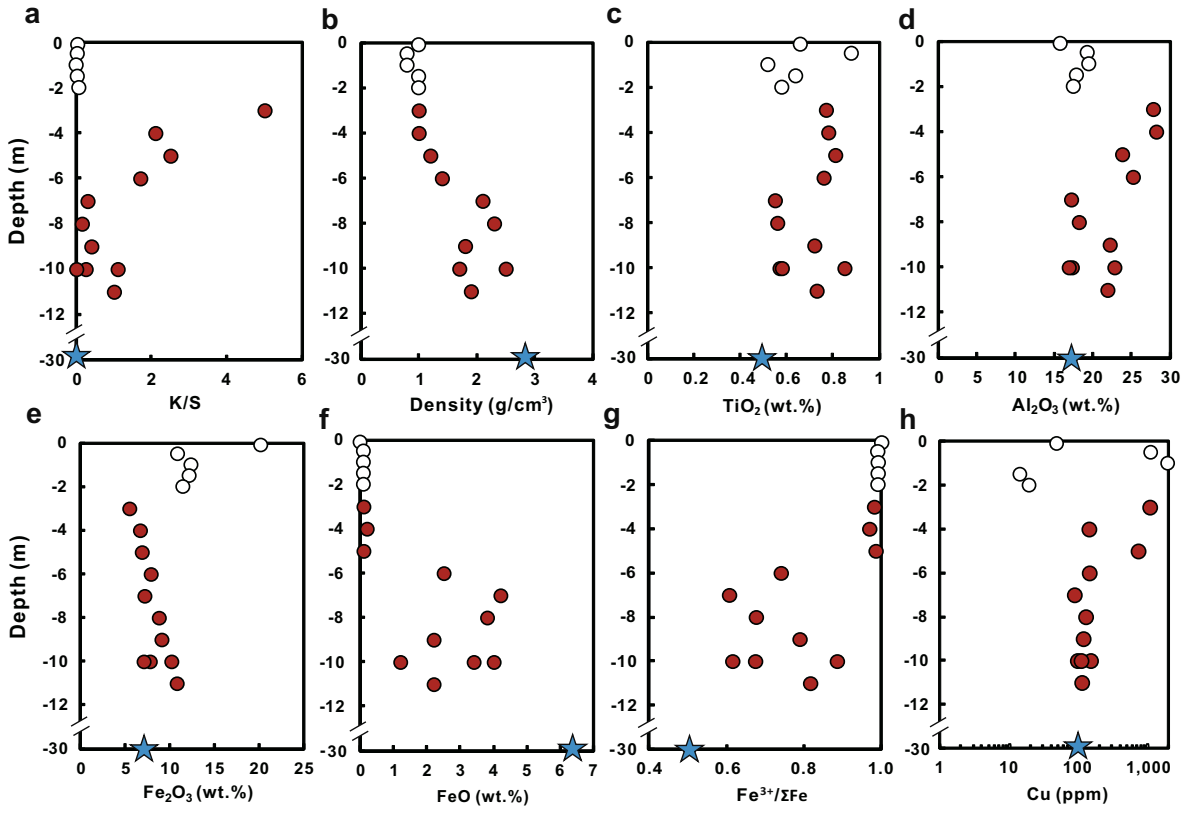

Fig. 1. kaolinite/smectite (K/S) ratio, bulk density and selected element concentrations of saprolites as a function of depth for the South Carolina profile. Star represents unaltered diabase. Open circles represent samples at or above 2 m depth and closed circles represent samples below 2 m. Data are reported in Table 2 and from Gardner et al. (1981). Cu concentrations were analyzed by solution ICP-MS in this study with typical uncertainty of ±10% (1σ).

from unaltered basalts at the bottom to an extremely weathered laterite residue towards the surface. The top soil and the gravel layer at the upper 50 cm were not sampled in order to avoid the disruption of farming activities. A set of fine laterite with a homogeneous red color developed beneath the gravel layer. Seven samples (HK06-01 to -07) were collected at intervals of 30 cm. Three samples (HK06-08 to -10) were sampled in the section from 250 to 320 cm depth. Below 320 cm, the soil color becomes pistachio with unaltered core stones, and nine samples were collected at intervals of 10–15 cm. In addition, the unaltered tholeiitic basalt sample (HK06-R1) was collected from 5 m below. The tholeiitic basalts erupted during the Neogene, and contain 10% of pyroxene in the phenocryst, and 60% of plagioclase, 25% of clinopyroxene and few opaque minerals in the groundmass (Ma et al., 2007).

The saprolites developed in the profile are dominated by secondary minerals, such as kaolinite, halloysite, gibbsite and Fe-oxy-hydroxides. Primary minerals are absent in the saprolites. A transition in clay mineralogy exists at 3 m depth of the weathering profile (Fig. 2). Beneath 3 m, the clay mineralogy is dominated by halloysite with modal abundances ranging from 30.7% to 87.4%, and kaolinite is absent except in the sample HK06-20 (20%). Above 3 m, kaolinite dominants the secondary mineral assemblage with modal abundances ranging from 28.3% to 82.0%, and only one sample (HK06-7) contains halloysite (53.4%). Other clay minerals, such as illites, are absent except in the sample HK06-7 that contains 16% illite (Ma et al., 2007).

Ma et al. (2007) found that the abundances of most elements, including major elements, rare earth elements (REEs) and immobile elements (Ti, Zr, Hf, Nb, and Ta) were significantly depleted above 3 m and gradually became enriched or less depleted in the section below 3 m. The depletion of REEs and immobile elements increases towards the surface, suggesting that weathering intensity increases towards the surface (Ma et al., 2007). CIA values (the chemical index of alteration) of saprolites in this profile are greater than 99%, and concentration of Al_2O_3 is up to 36 wt.%. These indicate that the chemical weathering intensity could be categorized as extreme (Nesbitt and Wilson, 1992). In addition, redox-sensitive elements such as Mn, Co, Ce, Cr and U are enriched in the middle profile, with maximum enrichment occurring at ~3 m. These enrichments are accompanied by significant depletion of total organic carbon and the absence of organic nitrogen, as well as higher water content in the middle profile. This suggests that organic colloids and redox conditions played an important role in transferring these elements during weathering (Ma et al., 2007). Studies of isotopic systematics with high masses such as Sr, Nd and Hf in the weathering saprolites found significant isotopic fractionations relative to the unaltered basalt, indicating extreme chemical weathering (Ma et al., 2010).

Twenty-one samples including one unaltered basalt and twenty saprolites from the Hainan profile were analyzed for Fe and Cu isotopes in this study. The mineralogy, major and trace element geochemistry, as well as Mg isotopes for these samples were previously reported (Ma et al., 2007; Huang et al., 2012).

3. ANALYTICAL METHODS

The detailed procedures for sample digestion, column chemistry and instrumental analysis in this study follow the methods of Liu et al. (2014). Only a brief description is given below.

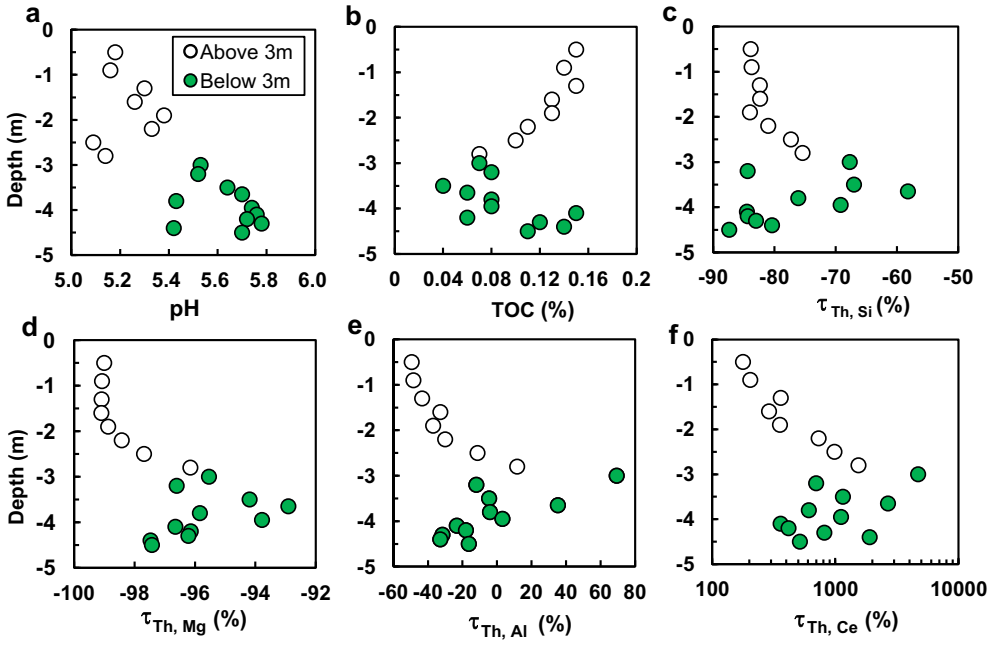

Fig. 2. Normalized element concentrations, pH values and total organic carbon (TOC) of saprolites as a function of depth for the Hainan profile. Data are from Table 4 and Ma et al. (2007).

3.1. Sample dissolution and chemical purification

The studied saprolites and unaltered basalt/diabase have Cu concentrations ranging from ~20 to >1000 ppm. Accordingly, 10–20 mg samples were weighted and digested to obtain at least 0.4 μg Cu and 20 μg Fe for high-precision Cu and Fe isotope analysis. After complete dissolution, 1 ml of 8 N HCl + 0.001% H_2O_2 was added to the beaker and then heated to dryness at 80 °C. This process was repeated three times and the final material was dissolved in 1 ml of 8 N HCl + 0.001% H_2O_2 in preparation for ion-exchange separation.

Copper and iron were purified by a single column ion-exchange chromatography using Bio-Rad strong anion resin AG-MP-1M (Liu et al., 2014). 2 ml pre-cleaned resin was loaded onto the cleaned column. Matrix elements were eluted in the first 10 ml 8 N HCl and Cu was collected in the following 24 ml of 8 N HCl. Then, 18 ml of 2 N HCl + 0.001% H_2O_2 was passed through the column to elute the iron fraction. The recovery for both Cu and Fe is >99.7%. The total procedural blanks are always <2 ng for Cu and <10 ng for Fe based on long-term analyses, which are considered negligible. The Cu and Fe fractions were evaporated to dryness, dissolved in 3% HNO_3, and then re-evaporated to dryness and re-dissolved in 3% HNO_3 to remove all chlorine prior to isotope analysis. Matrix Ti and Na were checked for each eluted Cu fraction because they are found to significantly impact the accuracy of Cu isotope analysis due to molecular spectral interference (Liu et al., 2014). Their ratios to Cu are negligible (<0.1%) for all samples after two times of column chemistry.

In addition, two saprolite samples (M7 and M11) with extreme Fe isotopic compositions from the South Carolina profile were also purified using the AG-X8 resin following the general method of Dauphas et al. (2009). The results agree well (within ±0.02‰) with those obtained by the present single-column procedure and further confirm that our single column purification of Cu and Fe could produce precise and accurate Fe isotope data (Liu et al., 2014).

3.2. Instrumental analysis

Copper and iron isotopic ratios were measured using the *Neptune plus* MC-ICP-MS at the Isotope Geochemistry Laboratory of the China University of Geosciences, Beijing. Standard-sample bracketing (SSB) method was used in order to correct for instrumental mass fractionation (Zhu et al., 2002; Schoenberg and von Blanckenburg, 2005; Borrok et al., 2007; Dauphas et al., 2009). External normalization using Zn or Ni as a spike is unnecessary here because it produced little improvement of precision and accuracy compared with the SSB method (Liu et al., 2014). A measurement consists of four blocks of 40 cycles of ~8 s each, and thus each value reported is average of 160 ratios. Cu isotopic data are reported in standard δ-notation in per mil relative to standard reference material (SRM) NIST 976. Iron isotopes were measured in high-resolution mode with mass resolution M/ΔM = ~10,000. ^{53}Cr was measured simultaneously to correct any ^{54}Cr interference on ^{54}Fe and the signal ratio of $^{53}Cr/^{54}Fe$ is at or below the level of 10^{-5}. Because Cr was undetected in the Fe faction after column chemistry, corrected results agree with the uncorrected values within ±0.02‰. Fe isotope data are reported in standard δ-notation in per mil relative to reference material IRMM-014.

The long-term external reproducibility for $\delta^{65}Cu$ and $\delta^{56}Fe$ measurements is better than ±0.05‰ (2SD) and ±0.049‰ (2SD), respectively, based on repeated analyses of natural samples and synthetic solutions (Liu et al., 2014). Several international rock standards (e.g., BHVO-2, BCR-2, BIR-1 and GSP-2) were analyzed for both Cu and Fe isotopes during the course of this study (Table 1). The results agree well with previous studies for Cu isotopes (Li et al., 2009; Bigalke et al., 2010a) and Fe isotopes (Carddock and Dauphas, 2010; Millet et al., 2012).

3.3. Sequential extraction of bulk soils from the South Carolina profile

In parallel, an aliquot of saprolite samples from the upper part of the South Carolina profile was subjected to a two-step extraction with 0.5 N HCl. The method was designed to operationally separate poorly-crystalline iron oxides from crystalline iron oxides and silicate-bound iron (e.g., Fantle and DePaolo, 2004; Wiederhold et al., 2007). Since saprolites from the entire Hainan profile have relatively homogeneous Fe isotopic compositions (see below), only samples from the South Carolina profile were subject to leaching. In detail, 5 ml of 0.5 N HCl was added to ~0.1 g of bulk soils in a PFA tube. The tubes were shaken vigorously for 24 h at room temperature (~20 °C) for sufficient reaction and centrifuged for 10 min, and then the supernatants were filtered and separated from the residues. The residues were completely dissolved by following the digestion procedure of bulk saprolites and basalt protoliths. Both the extracted solutions and residues were processed through column and measured for Fe isotopic ratios.

Table 1
Fe and Cu isotopic compositions of international rock standards analyzed in this study.

Sample type	Name	$\delta^{65}Cu$	2SD	n^a	$\delta^{56}Fe$	2SD	$\delta^{57}Fe$	2SD	n
Basalt, Hawaiian, USA	BHVO-2	0.13	0.06	4	0.11	0.04	0.22	0.04	4
Basalt, Iceland	BIR-1	−0.01	0.05	4	0.08	0.03	0.13	0.07	4
Basalt, USGS	BCR-2	0.22	0.05	4	0.11	0.03	0.17	0.01	3
Granodoirite, USA	GSP-2	0.32	0.05	4	0.17	0.03	0.25	0.07	4
Andesite, USA	AGV-2	0.10	0.04	4	0.11	0.04	0.18	0.03	4

2SD = 2 times the standard deviation of the population of n repeat measurements of a sample solution.
[a] The times of repeat measurements of the same purification solution by MC-ICP-MS.

Table 2
Major element composition, bulk density and Fe and Cu isotopic compositions of saprolites and unaltered diabase from South Carolina.

Sample	Depth (m)	Density g/cm^3	K/S	TiO_2 wt.%	Fe_2O_3B wt.%	Fe_2O_3E wt.%	FeO wt.%	$Fe^{3+}/\Sigma Fe$	$\tau_{Ti,Fe}$	Cu (ppm)	$\tau_{Ti,Cu}$	CIA	$\delta^{65}Cu$	2SD	$\delta^{56}Fe$	2SD	$\delta^{57}Fe$	2SD
M1	0.1	1	0.04	0.66	16.19	4.04	0.00	1.00	4.0	48.2	−65	88	0.75	0.05	0.37	0.07	0.61	0.07
M3	0.5	0.8	0.03	0.88	10.75	0.13	0.06	0.99	−57	1103	504	88	−1.22	0.09	0.77	0.05	1.20	0.07
M4	1	0.8	0	0.52	12.29	0.10	0.09	0.99	−18	1936	1694	92	3.63	0.06	0.72	0.05	1.06	0.05
Repeat													3.65	0.08	0.67	0.04	1.00	0.07
M5	1.5	1	0.03	0.64	12.04	0.19	0.08	0.99	−35	14.2	−89	90	0.62	0.03	0.72	0.03	1.02	0.05
M6	2	1	0.07	0.58	11.27	0.24	0.08	0.99	−32	19.3	−84	87	1.48	0.05	0.61	0.06	0.93	0.05
Repeat													1.55	0.07	0.60	0.03	0.90	0.09
M7	3	1	5	0.77	5.27	0.19	0.14	0.98	−75	1065	567	95	−0.17	0.03	0.92	0.03	1.35	0.02
Repeat															0.90	0.05	1.35	0.06
M8	4	1	2.1	0.78	6.45	0.16	0.16	0.97	−70	140.9	−13	95	0.03	0.03	0.87	0.06	1.27	0.06
M9	5	1.2	2.5	0.81	6.57	0.27	0.10	0.98	−71	723.7	331	93	0.24	0.06	0.75	0.04	1.08	0.06
M10	6	1.4	1.7	0.76	7.40	0.50	2.46	0.74	−52	142.6	−10	91	0.15	0.05	0.52	0.06	0.75	0.06
M11	7	2.1	0.3	0.55	6.75	0.49	4.15	0.61	−27	86.8	−24	54	0.63	0.07	−0.01	0.06	−0.05	0.04
Repeat															0.01	0.06	0.01	0.06
M12	8	2.3	0.15	0.56	7.89	0.92	3.80	0.68	−21	126.2	9.0	55	−0.01	0.04	0.07	0.06	0.11	0.06
Repeat													0.02	0.06	0.03	0.03	0.07	0.06
M13	9	1.8	0.4	0.72	8.52	0.61	2.21	0.79	−45	116.4	−24	71	0.14	0.06	0.27	0.04	0.38	0.06
M14	10	1.7	1.1	0.85	9.56	0.64	1.24	0.88	−54	148.7	−16	90	0.05	0.03	0.57	0.06	0.84	0.06
L14-8	10	2.5	0.25	0.57	6.87	0.89	3.39	0.67	−31	95.8	−19	49	0.10	0.04	0.11	0.04	0.17	0.05
L14-9	10	2.5	0	0.58	5.95	1.14	3.98	0.62	−32	108.4	−10	46	0.02	0.06	0.08	0.03	0.13	0.06
M15	11	1.9	1	0.73	10.09	0.71	2.18	0.82	−38	110.8	−27	88	0.04	0.05	0.38	0.03	0.60	0.06
M20	30	3	0	0.48	3.13	0.37	6.26	0.50	0.00	99.6	0.00	45	0.01	0.04	0.04	0.07	0.09	0.06

Sample M20 at 30 m depth is the unaltered diabase protolith. Depth, bulk densities, K/S and major element data are from Gardner et al. (1981), where K/S = kaolinite/smectite intensity ratios were analyzed from XRD and FeO concentration was determined by titration. CIA values are from Rudnick et al. (2004), which is molar $Al_2O_3/(Al_2O_3 + CaO^* + Na_2O + K_2O)$, where CaO^* refers to Ca that is not contained in carbonate and phosphate. Fe_2O_3B = bound Fe_2O_3; Fe_2O_3E = extractable Fe_2O_3 determined by sodium dithionite–citrate–bicarbonate. Ti-normalized $\tau_{Ti,Fe(Cu)}$, $100 \times [(X/Ti)_{saprolite}/(X/Ti)_{protolith} - 1]$, where X = Fe or Cu, is used to evaluate element mobility by assuming that Ti is most immobile during basalt weathering. Two samples (M-7 and M-11) with extreme Fe isotopic compositions are repeated using the general procedure following the method of Dauphas et al. (2009). Repeat indicates repeating sample dissolution, column chemistry and isotope ratio measurement.

Table 3
Fe isotopic compositions of leached mineral pools and residues by 0.5 N HCl for five bulk soils from the upper profile of the South Carolina profile.

Sample no.	Leached pools					Residue					Bulk soils (calculated)	
	Percent	δ^{56}Fe	2SD	δ^{57}Fe	2SD	Percent	δ^{56}Fe	2SD	δ^{57}Fe	2SD	δ^{56}Fe	2SD
M-1	0.73	0.46	0.04	0.71	0.06	0.27	−0.15	0.04	−0.21	0.07	0.30	0.04
M-3	0.29	0.61	0.05	0.94	0.07	0.72	0.88	0.05	1.37	0.06	0.80	0.05
M-4	0.15	0.17	0.05	0.26	0.07	0.85	0.79	0.04	1.22	0.06	0.69	0.04
M-5	0.13	0.10	0.05	0.15	0.05	0.87	0.78	0.05	1.18	0.05	0.69	0.05
M-6	0.19	0.02	0.05	0.04	0.08	0.81	0.77	0.06	1.15	0.08	0.62	0.06

The calculated Fe isotopic compositions of bulk soils were weighted mean of the leached mineral pools and residues. The calculated values are in agreement, within analytical uncertainty, with measured values of bulk soils reported in Table 2.

4. RESULTS

Fe and Cu isotopic compositions of the unaltered diabase and saprolites from the South Carolina profile are reported in Table 2. The Fe isotopic data for extracted solutions and residues are reported in Table 3. Fe and Cu isotopic compositions of the unaltered basalt and saprolites from the Hainan profile are reported in Table 4. All samples including geostandards analyzed in this study define the mass fractionation line in three-isotope space (δ^{57}Fe vs. δ^{56}Fe) with a slope of 1.484 ± 0.012 (1σ), indicating no analytical artifacts from unresolved isobaric interferences on Fe isotopes.

4.1. Fe and Cu concentrations and isotopic compositions of the South Carolina profile

The unaltered diabase has $\delta^{56}Fe = +0.04‰$, which falls within the range of global basaltic rocks (Beard et al., 2003a; Dauphas et al., 2010; Teng et al., 2013). The saprolites display a wide range of δ^{56}Fe from −0.01‰ to +0.92‰ ($n = 14$). This 0.93‰ variation is one of the largest (0.3–0.9‰) among various parts of different bulk soils worldwide (Fantle and DePaolo, 2004; Emmanuel et al., 2005; Thompson et al., 2007; Wiederhold et al., 2007). In detail, Fe isotopic compositions of the saprolites are either similar to or skewed towards heavier values relative to the unaltered diabase and display a discontinuity at 2 m (Fig. 3). Fe isotopic variation in the lower part (below 2 m) is much larger (0.93‰) than that in the upper part (0.39‰) (above 2 m). The proportion of Fe in the extracted mineral pools is 13–73% of Fe in the bulk soils. The mineral pools extracted by 0.5 N HCl are isotopically lighter than the bulk soils by 0.2–0.5‰, except for the upmost sample (M-1). Fe mineral pool of sample M-1 has a slightly heavier isotopic composition by ~0.09‰ than the bulk soil. The leached residues display heavy δ^{56}Fe values relative to the extracted pools for four soil samples, whereas the extracted residue of sample M-1 is enriched in light Fe isotopes. For all five samples, the bulk δ^{56}Fe values calculated from the weighted average of the extracted mineral pools and residues agree with measured values of bulk digests (Table 3).

The Ti-normalized concentration ($\tau_{Ti,\ X}$) can quantitatively evaluate the relative element mobility during chemical weathering of basaltic rocks (Nesbitt and Young, 1982), described as $\tau_{Ti,\ X} = 100 \times [(X/Ti)_{saprolite}/(X/Ti)_{protolith} - 1]$, where X = Fe or Cu. The saprolites in the lower part have $\tau_{Ti,Fe} = -75$ to -21 (Table 2), suggesting that about 21–75% of Fe was leached out of the profile during weathering. In the upper part, $\tau_{Ti,Fe}$ values vary from −57 to 4.0, suggesting that some samples underwent significant Fe loss but there was extraneous Fe for the sample closest the surface.

The unaltered diabase of the South Carolina profile has $\delta^{65}Cu = +0.01‰$. This value is consistent with values reported for igneous rocks, which are generally close to zero (Maréchal et al., 1999; Zhu et al., 2000; Li et al., 2009). δ^{65}Cu values of the saprolites range from −1.22‰ to +3.63‰ with an overall variation of up to 4.85‰, significantly larger than those previously reported in soil profiles (0.3–1.8‰) (Bigalke et al., 2010a, 2011; Mathur et al., 2012). Like Fe isotopes, Cu isotopes also show a clear discontinuity at 2 m, with saprolites below 2 m exhibiting less variation compared with those located above 2 m (Fig. 4a). Ti-normalized Cu concentration ($\tau_{Ti,Cu}$) of most samples located below 2 m is less variable and similar to that of the unaltered diabase. By contrast, over two orders of magnitude variation in $\tau_{Ti,Cu}$ values (−89 to 1694) is observed for saprolites above 2 m (Fig. 4b).

4.2. Fe and Cu concentrations and isotopic compositions of the Hainan profile

The unaltered tholeiitic basalt from the Hainan profile has $\delta^{56}Fe = +0.08‰$, falling within the range of global oceanic basalts (Teng et al., 2013). The saprolites display a narrow range of δ^{56}Fe values from +0.05‰ to +0.14‰ (Fig. 5a), which are indistinguishable from the parent basalt. Five samples closest to the surface seem to be isotopically heavier than samples below them, but the difference is barely beyond the analytical uncertainty. For the Hainan profile, relative mobility of elements is normalized to thorium (Th), since Th is the least mobile element during extreme weathering (Ma et al., 2007). The normalized Fe concentration ($\tau_{Th,Fe}$) of saprolites below 3 m is almost constant and similar to that of the unaltered basalt. Above 3 m, moderate variation of $\tau_{Th,Fe}$ occurs towards the surface.

δ^{65}Cu value of the unaltered tholeiitic basalt is +0.04‰, falling within the range of global igneous rocks. δ^{65}Cu values of the saprolites vary significantly from −0.18‰ to +0.31‰ over the entire profile (Fig. 6a). The samples at the bottom (4.3–4.5 m) are depleted in ^{65}Cu relative to the

Table 4
Major- and trace elements, pH, TOC and Fe and Cu isotopic compositions of saprolites and unaltered basalt from the Hainan Island, China.

Sample	Depth (m)	pH	TOC	Th (ppm)	Fe_2O_3T wt.%	$\tau_{Th,Fe}$	Cu (ppm)	$\tau_{Th,Cu}$	$\delta^{65}Cu$	2SD	$\delta^{56}Fe$	2SD	$\delta^{57}Fe$	2SD
HK06-1	0.5	5.18	0.15	9.2	23.48	−39.2	118	−55.7	−0.17	0.05	0.12	0.06	0.18	0.09
HK06-2	0.9	5.16	0.14	9.19	23.45	−39.2	120	−54.9	−0.12	0.04	0.12	0.04	0.17	0.01
HK06-3	1.3	5.30	0.15	8.58	22.69	−37.0	119	−52.1	−0.14	0.05	0.12	0.03	0.19	0.03
HK06-4	1.6	5.26	0.13	7.9	21.62	−34.8	124	−45.8	−0.14	0.04	0.12	0.04	0.18	0.09
HK06-5	1.9	5.38	0.13	7.83	24.4	−25.8	146	−35.7	−0.12	0.04	0.13	0.04	0.18	0.07
HK06-6	2.2	5.33	0.11	7.1	23.41	−21.5	158	−23.2	−0.10	0.05	0.07	0.05	0.10	0.05
HK06-7	2.5	5.09	0.10	5.86	20.97	−14.8	160	−5.8	−0.05	0.05	0.06	0.05	0.11	0.06
HK06-8	2.8	5.14	0.07	5.02	20.43	−3.1	144	−1.0	−0.04	0.05	0.08	0.05	0.12	0.05
Repeat									−0.08	0.04				
HK06-9	3	5.53	0.07	3.72	15.74	0.8	173	60.5	0.02	0.05	0.10	0.03	0.16	0.06
HK06-10	3.2	5.52	0.08	5.99	25.52	1.5	237	36.5	0.22	0.04	0.09	0.06	0.16	0.09
HK06-12	3.5	5.64	0.04	4.9	19.32	−6.1	229	61.2	0.32	0.05	0.09	0.06	0.14	0.06
HK06-13	3.65	5.70	0.06	3.87	15.23	−6.3	163	45.3	0.23	0.05	0.09	0.06	0.15	0.04
HK06-14	3.8	5.43	0.08	5.21	23.4	7.0	237	56.9	0.08	0.05	0.05	0.05	0.09	0.02
HK06-15	3.95	5.74	0.08	4.74	19.44	−2.3	185	34.7	0.11	0.05	0.11	0.03	0.18	0.07
HK06-16	4.1	5.76	0.15	6.37	27.23	1.8	236	27.8	0.08	0.05	0.08	0.03	0.12	0.08
HK06-17	4.2	5.72	0.06	5.97	27.62	10.2	362	109.2	0.29	0.06	0.11	0.04	0.15	0.06
Repeat									0.28	0.03				
HK06-18	4.3	5.78	0.12	6.81	27.65	−3.3	234	18.6	−0.01	0.05	0.14	0.06	0.22	0.07
HK06-19	4.4	5.42	0.14	6.7	23.74	−15.6	239	23.1	−0.10	0.05	0.08	0.05	0.18	0.05
HK06-20	4.5	5.70	0.11	6.58	27.04	−2.1	233	22.2	−0.12	0.05	0.08	0.05	0.15	0.08
Repeat									−0.10	0.04				
HK06-R1	–	–	–	2.46	10.33	0.00	71.3	0.00	0.04	0.05	0.08	0.05	0.12	0.07

Sample HK-6-R1 is the unaltered diabase protolith. Depth, pH, total organic carbon (TOC) and major-trace elements are from Ma et al. (2007). Th-normalized $\tau_{Th,X}$, $100 \times [(X/Th)_{saprolite}/(X/Th)_{protolith} - 1]$, where X = Fe or Cu, is used to evaluate element mobility by assuming that Th is most immobile during extreme weathering.

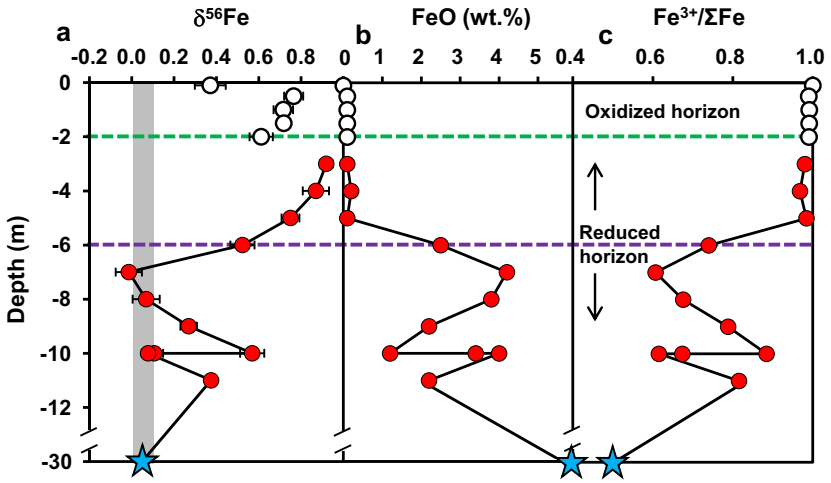

Fig. 3. Variation of $\delta^{56}Fe$ values (a), FeO contents (b) and $Fe^{3+}/\Sigma Fe$ (c) of saprolites from the South Carolina profile as a function of depth. Symbols are same as in Fig. 1. The two dashed lines denote two possible discontinuities at depths of 2 m and 6 m, respectively. The 2 m depth denotes a boundary of redox condition with the upper part oxidized and the lower part reduced (Gardner et al., 1981).

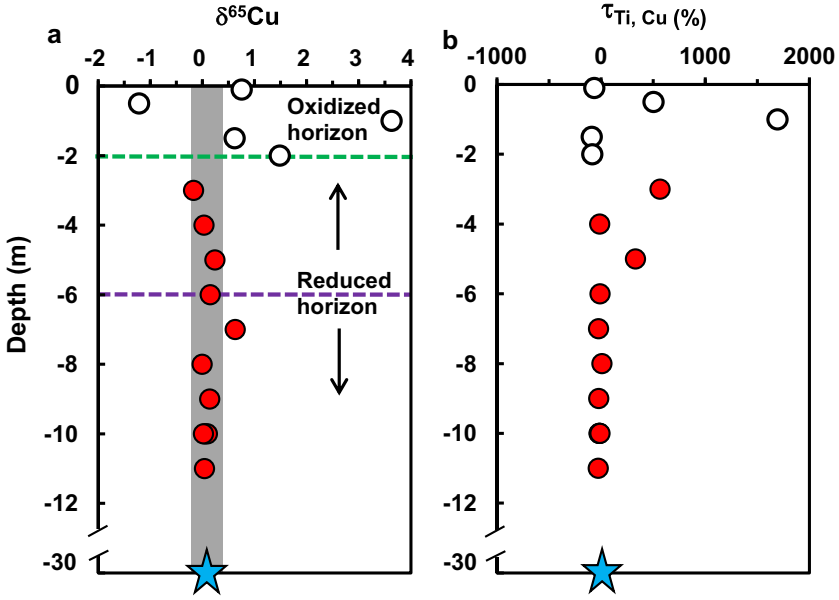

Fig. 4. Variation of Cu isotopic compositions and normalized Cu concentrations of saprolites from the South Carolina as a function of depth. The dashed line denotes the 2 m depth discontinuity. Symbols are same as in Fig. 1. The error bars of $\delta^{65}Cu$ values are smaller than the symbol size. Data are reported in Table 2.

unaltered basalt, but increase upwards from 4.3 to 3 m. Above 3 m, $\delta^{65}Cu$ values progressively decrease towards the surface (Fig. 6a). The Cu isotopic variation over the entire profile depth is highly coupled with Cu concentration variation (Fig. 6b). For example, $\tau_{Ti,Cu}$ values increase from the bottom to 3 m and then decrease towards the surface.

5. DISCUSSION

In this section, we first discuss the possible mechanisms and processes causing Fe and Cu isotopic variations in these two weathering profiles. Then, we discuss the potential implications of Fe and Cu isotopes for tracing redox condition, paleoclimate and biological cycling during weathering and pedogenic translocation based on observations from the present study.

5.1. Iron isotope fractionation during weathering and pedogenesis

The South Carolina profile provides an opportunity for studying Fe isotope fractionation during continental weathering at different redox regimes because the upper and lower parts of this profile were formed at different redox conditions. The lower part of the South Carolina profile (below 2 m) was formed under reduced condition as

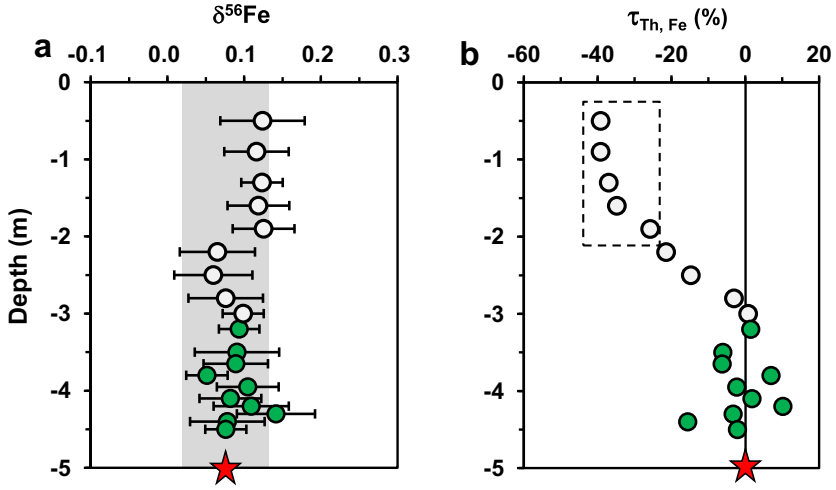

Fig. 5. The variation of Fe isotopic compositions and normalized Fe concentrations of saprolites from the Hainan profile as a function of depth. Fe isotopic data are reported in Table 4 and Fe concentration data are from Ma et al. (2007).

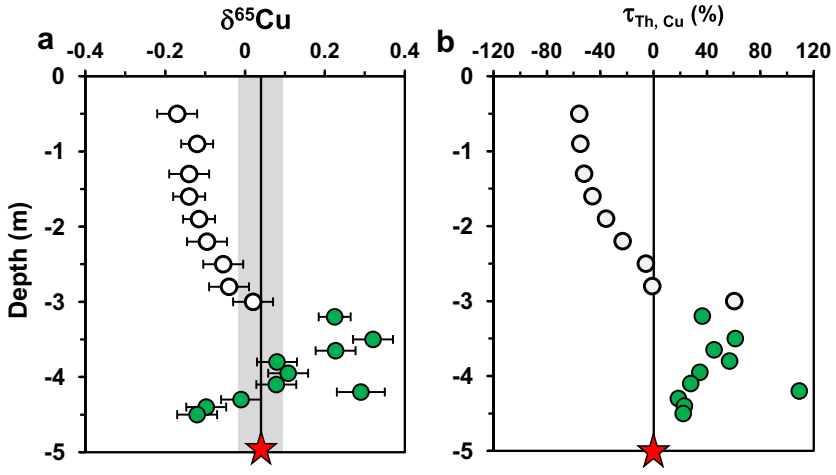

Fig. 6. The variation of Cu isotopic compositions and normalized Cu concentrations of saprolites from the Hainan profile as a function of depth. Cu isotopic data are reported in Table 4 and Cu concentration data are from Ma et al. (2007).

evidenced by the occurrence of siderite (Gardner et al., 1981). As shown in Fig. 7, δ^{56}Fe values of saprolites in this part are positively correlated with $Fe^{3+}/\Sigma Fe$ ($R^2 = 0.90$) and the chemical index of alteration (CIA) ($R^2 = 0.84$), and negatively correlated with FeO contents ($R^2 = 0.93$) and $\tau_{Ti,Fe}$ values ($R^2 = 0.95$). Two important conclusions can be drawn from these correlations. First, Fe was significantly lost from the profile, which is closely associated with the weathering intensity, and Fe^{2+} was preferentially removed relative to Fe^{3+}. Second, light Fe isotopes were released to solutions with heavy Fe isotopes preferentially left in the weathered residues. The results thus provide the most direct evidence, based on natural observations, that Fe isotope fractionation during silicate weathering is redox-controlled.

Two completely different mechanisms have been proposed to explain the behavior of Fe isotope fractionating during weathering: (i) uptake of Fe from a single mineral with organic ligands and (ii) preferential decomposition of isotopically distinct phases. A combined effect of formation of the Fe-depleted layer of the silicate surface, uptake of isotopically heavy ferric Fe from solution by bacterial cells and preferential adsorption of isotopically light Fe^{2+} onto mineral was proposed to explain the light isotopic compositions of leaching Fe relative to starting hornblende (Brantley et al., 2004). Alternatively, leaching experiments of biotite granite and basalt using hydrochloric and oxalic acids indicate that Fe initially released into solution was isotopically light due to dissolution of chlorite and pigeonite, respectively (Chapman et al., 2009). A similar mechanism, relying on potential isotopic difference among solid phases of the parent rocks, has also been proposed for Mg isotope fractionation during granite dissolution (Ryu et al., 2011). The unaltered diabase from the South Carolina profile contains significant amounts of ferrous phases such as chlorite (8%), which was weathered prior to pyroxene (Gardner et al., 1981). Consequently, our results favor the explanation that initial dissolution of chlorite followed

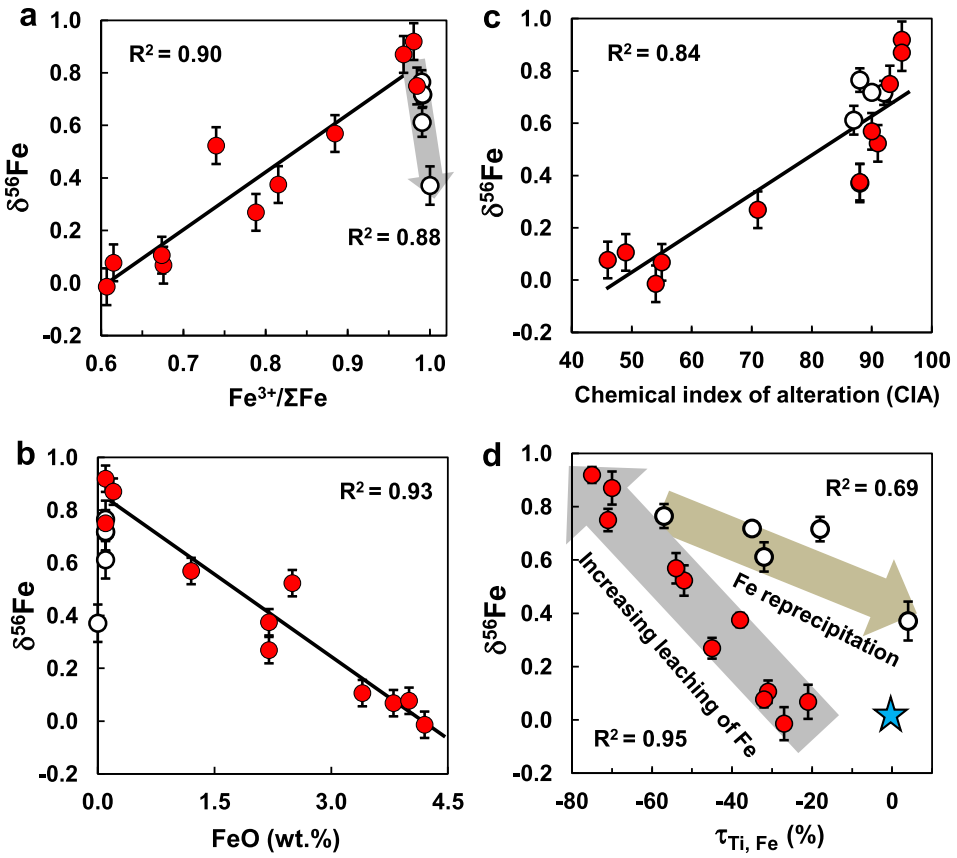

Fig. 7. Correlation of $\delta^{56}Fe$ with $Fe^{3+}/\Sigma Fe$, FeO concentrations, chemical index of alteration (CIA) and $\tau_{Ti,Fe}$ values for the saprolites from the South Carolina profile. The data are from Table 2 and Gardner et al. (1981).

by pyroxene may rapidly release isotopically light Fe^{2+} into the solutions and leave isotopically heavy Fe in the residue (e.g., Kiczka et al., 2010).

Previous studies reported significant Li and Mg isotope fractionation in the South Carolina profile (Rudnick et al., 2004; Teng et al., 2010). As weathering intensity increases and density decreases towards the surface, Mg isotopes become progressively heavier whereas Li isotopes get lighter relative to the unaltered diabase. These results are generally consistent with the release of isotopically light Mg or heavy Li into porewater during weathering as observed from river waters (Huh et al., 1998; Tipper et al., 2006). However, unlike Fe, concentrations and isotopes of both Li and Mg show no discontinuity at the depth of 2 m that marks the redox boundary within the profile (Rudnick et al., 2004; Teng et al., 2010). This difference further manifests that redox conditions and formation of secondary Fe-bearing phases (see below) plays a key role in fractionating Fe isotopes during weathering.

The Fe isotopic variation in the Hainan profile is much smaller than the South Carolina profile (Fig. 5a). Most samples display limited variation in Fe concentrations ($\tau_{Th,Fe} = \pm 20\%$) compared to the reduced part of the South Carolina profile (−75% to −21%), although five samples above 2 m have moderately negative $\tau_{Th,Fe}$ (−39% to −26%) that are similar to the oxidized part of the South Carolina profile. Given the extreme weathering under oxidized condition, Fe would be transformed into immobile ferric Fe and can be re-precipitated as Fe (hydr)-oxides as observed in the Hainan profile where gibbsite and Fe (hydr)-oxides dominate the major Fe phases (Ma et al., 2007). The five samples with moderately negative $\tau_{Th,Fe}$ values undergone significant Fe lost and have slightly heavy $\delta^{56}Fe$ values similar to saprolites from the South Carolina profile in same $\tau_{Th,Fe}$ values, which also indicates redox-controlled Fe isotope fractionation during weathering. Nevertheless, the limited Fe isotopic variation over the whole profile suggests that extreme weathering induces limited Fe isotope fractionation.

After primary mineral dissolution, secondary processes may also further affect Fe isotopic compositions of the saprolites. Iron isotopic variation of saprolites at above 2 m (oxidized part) is smaller than that at below 2 m (reduced part) in the South Carolina profile (Fig. 3). In addition, $\delta^{56}Fe$ values of saprolites suddenly decrease towards the surface across the 2 m discontinuity but the values are still heavier than the unaltered diabase. All samples above 2 m except the one closest to the surface have $\tau_{Ti,Fe}$ values that are significantly negative (−57% to −18%). The heavy Fe isotopic compositions of saprolites above 2 m relative to the unaltered diabase and negative $\tau_{Ti,Fe}$ values indicate loss of isotopically light Fe(II). However, this process seems unlikely to explain the negative relationship of $\delta^{56}Fe$ with $Fe^{3+}/\Sigma Fe$ ($R^2 = 0.88$) (Fig. 7a)

because it predicts that heavy $\delta^{56}Fe$ should positively correlate with elevated $Fe^{3+}/\Sigma Fe$ as observed in the lower part (below 2 m), if Fe isotopic variation is mainly a result of redox transformation. Additional processes must have affected samples in the upper part.

The negative relationship of $\delta^{56}Fe$ with $Fe^{3+}/\Sigma Fe$ and $\tau_{Ti,Fe}$ values above 2 m indicates the addition of Fe with light isotopic compositions, e.g., re-precipitated Fe from waters or soil solutions. This is strongly supported by the fact that the sample closest to the surface has positive $\tau_{Ti,Fe}$ value (4.0) relative to the unaltered diabase. This hypothesis is also confirmed by sequential leaching of bulk soils which allows analysis of Fe isotopic compositions of different Fe fractions in soils without inducing Fe isotope fractionation (Fantle and DePaolo, 2004; Emmanuel et al., 2005; Wiederhold et al., 2007; Bigalke et al., 2011). The Fe mineral pools of saprolites from the upper part of the South Carolina profile extracted by 0.5 N HCl, representing the poorly-crystalline Fe oxides, are isotopically lighter than the bulk soils (Fig. 8) except for the sample closest to the surface (M-1). This demonstrates that saprolites in the upper profile contain isotopically light, poorly-crystalline Fe hydr-oxides. The formation of poorly-crystalline Fe hydr-oxides in the upper profile was suggested to have resulted from oxidation of the formerly existed siderite in the soils to Fe^{3+} ions and precipitation (Gardner et al., 1981). Siderite generally has light Fe isotopic composition because it is precipitated from groundwater or soil solutions and Fe isotope fractionation between $Fe(II)_{aq}$ and siderite is positive: $10^3 \ln\alpha_{Fe(II)\text{-}Siderite} = +0.48‰$ at 20 °C (Wiesli et al., 2004). The Fe^{3+}-bearing phases are also enriched in light Fe isotopes similar to the original siderites, which were mixed with other parts of the saprolites to produce the light Fe isotopic signatures across the 2 m discontinuity. Collectively, these additional processes could have contributed to a greater extent of Fe isotope fractionation after primary mineral dissolution.

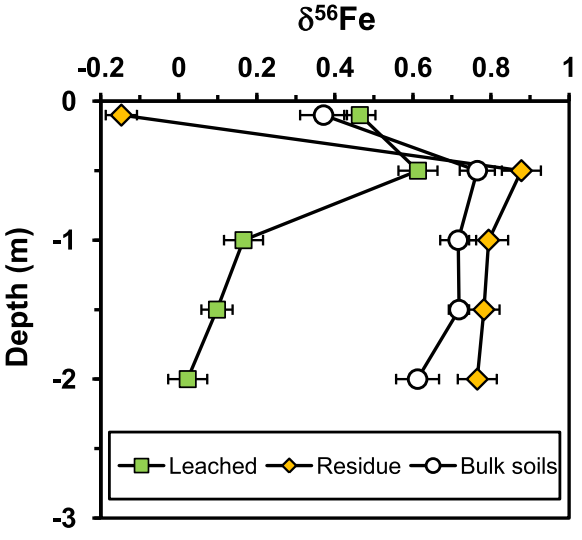

Fig. 8. The variation of $\delta^{56}Fe$ values of extracted Fe mineral pools and residues of the saprolites from the upper part of the South Carolina profile (above 2 m) as a function of depth. Data are reported in Table 3.

It is noteworthy that the Fe mineral pool extracted from sample M-1 has heavier $\delta^{56}Fe$ than the bulk soil (Fig. 8). 73% of total Fe has been leached from the sample compared to other samples (13–29%). There is thus a minor component in this sample that is isotopically light and is resistant to dissolution by 0.5 N HCl. This component may be organic if the organically-bound Fe is isotopically light (e.g., Brantley et al., 2001). Such a feature has been previously observed by Fantle and DePaolo (2004) but rarely observed in most of soil studies (e.g., Emmanuel et al., 2005; Wiederhold et al., 2007; Bigalke et al., 2011). Wiederhold et al. (2007) argued that the treatment of bulk soils at 600 °C to destroy organic matter as done in Fantle and DePaolo (2004) may also change the Fe mineralogy of the soil sample and thus influence the leaching data. Our samples of saprolites were not treated by similar procedure and the results might thus confirm that organic matters with isotopically light Fe relative to poorly-crystalline Fe oxides and silicate-bound iron can exist after extraction by 0.5 N HCl.

5.2. Copper isotope fractionation during weathering and pedogenesis

The variation of Cu concentration with depth is coupled with the variations of major elements such as Si, Mg and Al, and redox-sensitive trace elements such as Ce in the Hainan profile (Fig. 2). Given that saprolites in this profile formed under wet conditions, high rainfall occurred in association with formation of halloysite, Fe-oxides and kaolinite. Above 3 m, rainfall resulted in downward transformation of elements and formation of an enriched layer in the middle profile (~3–4 m) that was highly oxidized (Ma et al., 2007). The successive downward decrease of total organic carbon (TOC) above 3 m is also in association with the remarkable change of redox condition, as a result of decomposition of organic colloids in the oxidized layer. In addition, the presence of organic ligands during oxic conditions could enhance the mobilization of Cu because Cu forms strong complexes with chelating ligands (Neaman et al., 2005). The variations of both Cu (Si, Mg and Al, etc.) concentrations and the contents of TOC with depth can thus be due to redox-controlled transformation (Ma et al., 2007). Such a process can cause significant Cu isotope fractionation.

The positive correlation of $\delta^{65}Cu$ with $\tau_{Ti,Cu}$ values in the Hainan profile (Fig. 9a) indicates that Cu leached out of the profile is enriched in heavy Cu isotopes and the weathered residues are isotopically light. In detail, the increased $\delta^{65}Cu$ with depth above 3 m reflects the downward transformation of desorbed Cu, which is isotopically heavier than the organically-bound Cu. This transformation resulted in the enrichment of heavy Cu isotopes in the middle profile (3–4 m) and depletion in the upper profile (above 3 m). This can happen as the organic ligands are decomposed under oxidized condition and decreasing pH value towards the surface, which resulted in desorption (Fig. 2). The negative correlation of $\delta^{65}Cu$ values with the contents of TOC (Fig. 9b) in the Hainan profile indicates Cu isotope fractionation between organic ligand-bound Cu and dissolved (desorbed) Cu with the former isotopically lighter than the

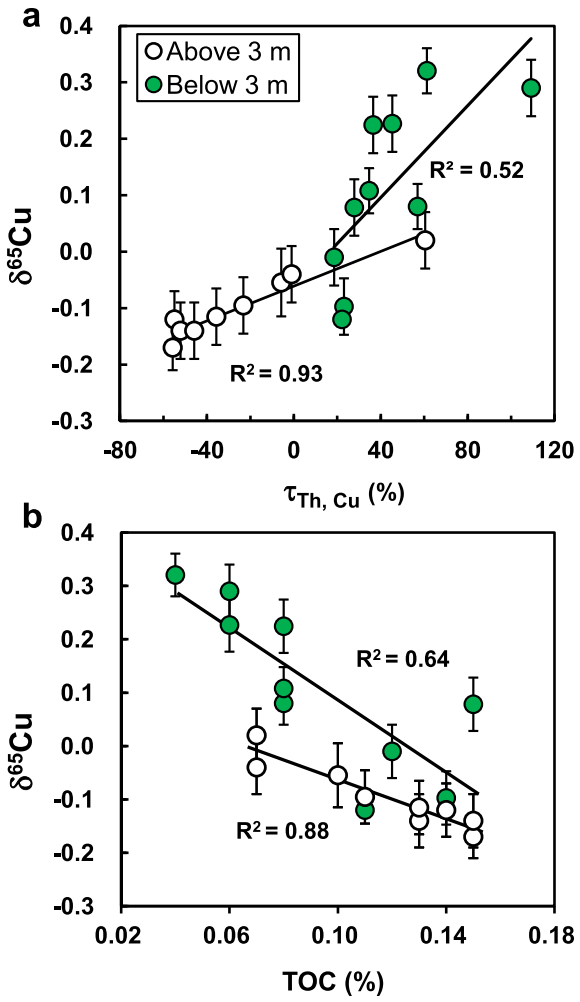

Fig. 9. Correlation of $\delta^{65}Cu$ with total organic carbon (TOC) and normalized Cu concentrations for the Hainan profile. Data are from Table 4 and Ma et al. (2007).

latter. This results in depletion of heavy Cu isotopes in the organic carbon-enriched layer (above 3 m) and enrichment in the organic carbon-depleted, oxidized horizon (~3 m). These observations are consistent with previous studies suggesting that biological processes can fractionate Cu isotopes in soils (Brantley et al., 2004; Mathur et al., 2005; Bigalke et al., 2011).

Below 3 m, $\delta^{65}Cu$ values decrease with depth towards the bottom of the profile, which is in contrast to the trend seen at above 3 m. Copper isotopic compositions are negatively correlated with pH values and the contents of TOC (Fig. 9a). Generally, increases of pH can improve the adsorption potential for cations onto the solid phases. Copper can be strongly absorbed onto the surface of negatively charged clay minerals (Dube et al., 2001). Experimental studies show that heavier Cu isotope preferentially adsorbs onto Fe hydr-oxide surface (Balistrieri et al., 2008; Pokrovsky et al., 2008). All samples below 3 m have positive $\tau_{Ti,Cu}$ values and most of them have heavy Cu isotopic compositions (Fig. 6), probably indicating preferential adsorption of heavy Cu isotopes onto Fe hydr-oxides (gibbsite, ilmenite and goethite). The decreased $\delta^{65}Cu$ and Cu concentration with depth at below 3 m may be explained as progressive decrease of dissolved, isotopically heavy Cu from upper profile with the distance to the surface, leaving the organic-rich soils enriched in light Cu isotope (^{63}Cu) with depth.

Huang et al. (2012) found that Mg isotopic compositions increase with depth above 3 m and decrease with depth below 3 m in the Hainan profile, which is very similar to Cu isotopic variation in the profile. Thorium-normalized Mg concentration also displays similar variation to $\delta^{26}Mg$ values. The variations of Mg concentration and isotopic compositions were interpreted as adsorption and desorption processes: adsorption of Mg to kaolin minerals, with preferential uptake of heavy Mg isotopes onto kaolin minerals; and desorption of Mg through cation exchange of Mg with the relatively lower hydration energy cations in the upper profile. Although $\delta^{65}Cu$ values show similar variation with the proportions of kaolin minerals in saprolites of the Hainan profile (Fig. 10), the correlation is much weaker than the correlation between $\delta^{65}Cu$ and TOC (Fig. 9b). Thus, although Cu adsorption onto clay minerals and desorption may fractionate Cu isotopes, biological cycling plays an important role in governing the Cu isotopic variation over the profile depth.

The overall variation of Cu isotopes (>4.8‰) in the South Carolina profile is the largest among soil profiles reported to date. The range of $\delta^{65}Cu$ (0.82‰) in the lower part (above 2 m) is much narrower than that in the upper part (4.85‰) (Fig. 4a). The Cu concentration variation is also different between the upper and lower profiles, with the upper profile two orders of magnitude ($\tau_{Ti,Cu} = -89$ to 1649) larger than that in the lower profile ($\tau_{Ti,Cu} = -27$ to 567) (Fig. 4b). Most of samples in the upper profile have high Cu concentrations (up to 1936 μg/g), which are similar to or even higher than those of contaminated soils (Bigalke et al., 2010a), indicating significant addition of Cu. Such an enrichment of Cu concentrations may be anthropogenic contamination such as contribution of smelters. Re-precipitation or adsorption of Cu onto Fe hydr-oxides could also increase Cu concentrations of the saprolites. Four out of five samples in the upper part of the South Carolina profile have positive $\delta^{65}Cu$ whereas one sample at 0.5 m has negative $\delta^{65}Cu$ (−1.22‰). This is similar to three zones with different Cu isotopic composition in porphyry deposits: the leach cap (oxidized zone) depleted in ^{65}Cu, enrichment blanket enriched in ^{65}Cu and hypogene zone with ^{65}Cu close to zero or the average of igneous rocks (Mathur et al., 2009). In general, soils have depleted $\delta^{65}Cu$ values as a result of oxidative weathering (Mathur et al., 2005, 2012; Fernandez and Borrok, 2009) during which isotopically heavy Cu^{2+} was dissolved and released into solutions (Bermin et al., 2006; Vance et al., 2008; Mathur et al., 2012). Although most soils are depleted in $\delta^{65}Cu$, soils enriched in ^{65}Cu were also reported (Bigalke et al., 2010a). Notably, the large Cu isotopic variation and heavy $\delta^{65}Cu$ in the upper profile is much different from the small variation and light $\delta^{65}Cu$ in the Hainan profile.

The different Cu isotopic patterns in these two studied profiles may be due to different climatic conditions under

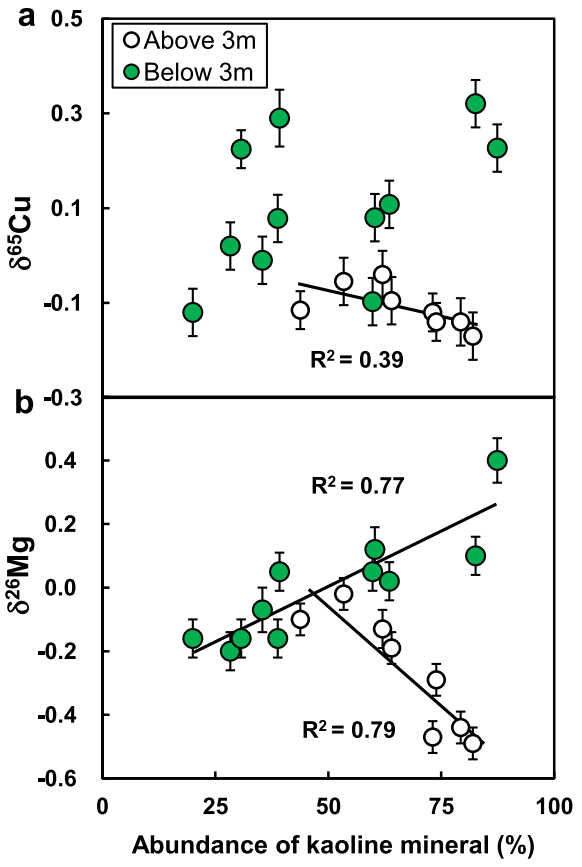

Fig. 10. Correlation of $\delta^{65}Cu$ and $\delta^{26}Mg$ with the abundance of kaolin minerals for the Hainan profile. The abundances of kaolin minerals are from Ma et al. (2007). $\delta^{26}Mg$ data are from Huang et al. (2012). Cu isotope data are reported in Table 4.

which the soils formed. The Hainan profile developed at a tropical climate with high rainfall and high contents of organic carbon, hence adsorption is relatively weak and downward transformation of desorbed Cu resulted in light Cu isotopic composition in the upper part (above 3 m). By contrast, at a subtropical climate in the South Carolina, adsorption is relatively strong and results in extreme enrichment of Cu concentration and heavy Cu isotopes of some saprolites in the upper profile (above 2 m). This is supported by experimental studies that heavy Cu isotopes are preferentially adsorbed onto Fe (hydr)-oxides with $\delta^{65}Cu_{solid} - \delta^{65}Cu_{solution}$ at +1‰ (Balistrieri et al., 2008; Pokrovsky et al., 2008). The saprolites in the upper part of the South Carolina (above 2 m) are enriched in Fe_2O_3 as a result of rapid transformation of kaolinite and siderite to Fe^{3+}-rich smectite and Fe hydr-oxides. Therefore, Cu re-precipitation from surface waters and/or soil solutions and adsorption onto Fe hydr-oxides may explain the heavy Cu isotopic signatures of saprolites in the upper profile.

5.3. Implications for using Fe and Cu isotopes as geological and biological tracers

Isotope geochemistry of Fe has gained particular interest due to its multiple redox states, which makes Fe isotopes widely used as redox indicator of ancient weathering environments. Nevertheless, most of post-Archean sedimentary rocks have $\delta^{56}Fe$ values that are close to the average of igneous rocks (Beard et al., 2003a; Beard and Johnson, 2004). Especially, despite large changes in $Fe^{3+}/\Sigma Fe$ ratios and thus redox condition, bulk sedimentary detritus remains unchanged in its $\delta^{56}Fe$ values in modern (oxygenated) environments (Yamaguchi et al., 2005). This relatively uniform $\delta^{56}Fe$ distribution reflects the very low solubility of Fe^{3+}-oxide minerals, which makes Fe act as a conservative element and difficult to be lost through fluid-mineral interactions, resulting in no change in Fe isotopic compositions in the weathering products (Beard et al., 2003b).

Compared with sedimentary rocks, redox conditions often change at short intervals and on a small scale in soils. Therefore, significant bulk-rock Fe isotopic variation was commonly observed in soil profiles (Fantle and DePaolo, 2004; Emmanuel et al., 2005; Wiederhold et al., 2007; Bigalke et al., 2011). However, Fe isotopic variation in soils may involve multiple processes including reductive dissolution, precipitation and biological cycling. It is therefore difficult to unambiguously fingerprint the role of each process. Our observations in the South Carolina profile strongly suggest that Fe isotope fractionation during basalt weathering is redox-controlled. Significant Fe isotopic variation can occur during mineral dissolution at reduced conditions and the magnitude of isotopic variations can be quantitatively related to the redox states in an isolated system. The linear variation of $\delta^{56}Fe$ values with the ratios of $Fe^{3+}/\Sigma Fe$ observed in the South Carolina profile (Fig. 7a) has crucial implications for Fe isotopes to be used as a predictor of long-term redox conditions, which are difficult to assess otherwise.

Like Fe, redox transformations between Cu(I) and Cu(II) species are also the principal process that fractionates Cu isotopes in natural systems (Zhu et al., 2002; Ehrlich et al., 2004). This nature of Cu evokes the great potential for using Cu isotopes as redox tracers in natural environments. However, Cu can be strongly adsorbed onto clay minerals or iron hydr-oxides relative to Fe (Dube et al., 2001), which strongly depends on solution pH values and much weakly depends on redox condition. In Fig. 11, we summarized published Cu isotope data for rivers and oceans (Vance et al., 2008), porewater (Mathur et al., 2012), soils (Bigalke et al., 2011; Mathur et al., 2012) and contaminated soils (Bigalke et al., 2010a). Rivers and oceans generally have positive $\delta^{65}Cu$ values relative to igneous rocks, probably due to preferential release of heavy Cu isotopes during continental weathering (Mathur et al., 2012). By contrast, $\delta^{65}Cu$ values of soils are not always light as expected and exhibit a large range with both positive and negative values. The heavy $\delta^{65}Cu$ values in soils may be attributed to adsorption as observed from contaminated soils (Bigalke et al., 2010a) as well as to re-precipitation from waters or soil solutions as observed from the South Carolina profile in this study.

In sharp contrast to the South Carolina profile, the Hainan profile exhibits much smaller Cu isotopic variation over depth and most samples in the upper part (above 3 m) have light Cu isotopic compositions. This difference indicates that

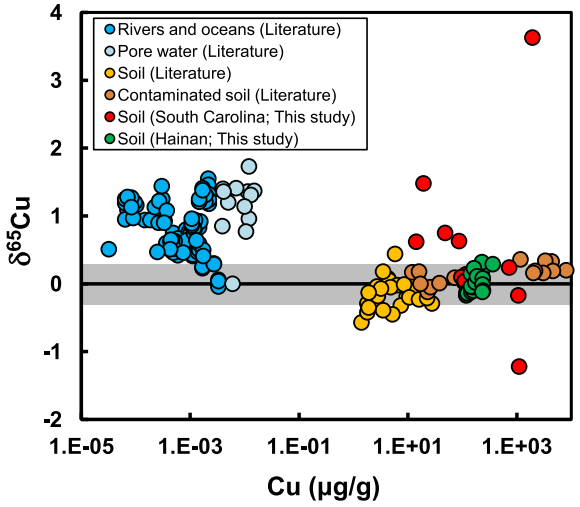

Fig. 11. A summary of Cu concentrations and isotopic compositions for seawater, river water, porewater and soils. The grey area represents the range of igneous rocks (Li et al., 2010). Data sources: rivers and oceans (Vance et al., 2008), pore water (Mathur et al., 2012), soils (Bigalke et al., 2011; Mathur et al., 2012), contaminated soils (Bigalke et al., 2010a). Data of soils from the South Carolina and Hainan profiles are from Tables 2 and 4.

Cu mobility and re-precipitation were probably favored by different climatic conditions. For example, at tropical climate re-precipitation is likely difficult to take place and desorption is strong due to high rainfall, resulting in isotopic depletion in the upper part of soil horizons. In summary, different climatic conditions may favor different capacity of adsorption as well as the development of organism, both inducing significant and distinct Cu isotope fractionation. The contrasting Cu isotopic signatures in the upper parts of these two studied profiles formed at different climatic conditions (subtropical vs. tropical) may have implications for using Cu isotopes to trace the ancient climate.

Previous studies have demonstrated that biological processes could significantly fractionate Cu isotopes. For example, Cu isotope fractionation has been observed during adsorption of Cu onto cell surfaces, co-precipitation and adsorption onto the mineral coatings (Mathur et al., 2005; Kimball et al., 2009; Navarrete et al., 2011). Zhu et al. (2002) observed Cu isotope variation during its incorporation into proteins synthesized by bacteria and yeast. Consistent with the results from previous Cu isotope studies on soils, our results indicate that complexation of Cu by organic matters is a key step for Cu isotope fractionation in the development of soils. Even in Cu-rich soils (>100 μg/g) formed by weathering of basalt in the Hainan profile, we observed that biological effects still played a key role in Cu transformation and isotope fractionation. This reveals the great potential of using Cu isotopes as a tracer of biological cycling, although further studies focusing on Cu isotope fractionation during adsorption on clay minerals and chemical reduction and reoxidation of soils are needed to improve our knowledge about the behaviors of Cu isotopes during long-term pedogenic processes.

6. CONCLUSION

We reported a comparative study of stable Fe and Cu isotopic ratios of saprolites developed on a diabase dike from South Carolina (USA) and on a basalt profile from Hainan Island (China), which formed under different climatic conditions. The results allow a detailed investigation of the behaviors of Fe and Cu isotopes during chemical weathering and pedogenic transformation at different redox and climatic conditions as well as at different amounts of organic matters. Several important points concluded from these observations are summarized below:

Firstly, large (up to 0.93‰) δ^{56}Fe variation was observed in the reduced part of the South Carolina profile, which is positively correlated with $Fe^{3+}/\Sigma Fe$ and CIA and negatively correlated with FeO concentrations and $\tau_{Ti,Fe}$. These results provide the most direct evidence from natural observations that Fe mobility and isotope fractionation during weathering is redox-controlled. This may have important potentials for using Fe isotopes as redox tracers for long-term soil formation processes.

Secondly, re-precipitation of Fe from waters or soil solutions can further result in Fe isotopic variation in bulk soils after primary mineral dissolution. This is supported by the negative correlation between δ^{56}Fe and $Fe^{3+}/\Sigma Fe$ in the oxidized part of the South Carolina profile and is demonstrated by our leaching experiments that Fe mineral pools extracted by 0.5 N HCl, representing the poorly-crystalline Fe (hydr)-oxides, are generally isotopically lighter than the bulk soils. Nevertheless, the extracted Fe mineral pools of one sample closest to the surface is isotopically heavier than the bulk soil, likely indicating organic complexing of Fe in this sample.

Thirdly, systematic Cu isotopic variation occurs in the Hainan profile formed under wet conditions with high rainfall, in contrast to the uniform Fe isotopic composition over the whole profile. The Cu isotopic variation with depth is coupled with Cu concentration and reflects downward transformation of desorbed/dissolved Cu that is enriched in heavy isotope. The organically-bound Cu is enriched in light Cu isotope relative to dissolved Cu as demonstrated by the positive correlation of δ^{65}Cu with the contents of TOC. This implies that ad/desorption and biological processes controlled Cu isotopic variation during weathering and soil formation, which has potential implications for using Cu isotopes as tracers of biogeochemical cycling.

Fourthly, saprolites in the upper part (above 2 m) of the South Carolina profile exhibit large Cu isotopic variation with most samples being isotopically heavy, which is in contrast to the small Cu isotopic variation and light isotopic signature in the upper part (above 3 m) of the Hainan profile. This difference indicates that Cu isotopic patterns in the upper parts of soil profiles were probably favored by different climatic conditions, under which rainfalls resulted in Cu desorption, transformation downward and re-precipitation. Therefore the different Cu isotopic patterns in saprolite profiles formed at different climatic conditions may have implications for using Cu isotopes to track the paleoclimate change.

Finally, our results show that although both Fe and Cu are redox-sensitive, they behave differently during redox-related weathering processes. These differences result in different dependence of Fe and Cu isotopes on weathering intensity, redox conditions and biological effects. Therefore, the combined utilization of Fe and Cu isotopes may be more efficient in fingerprinting the unique processes involved in weathering and pedogenesis compared with single isotopic systematics.

ACKNOWLEDGEMENT

We are grateful to Drs. Roberta Rudnick and Bob Gardner for sharing saprolite samples from the South Carolina weathering profile. Shan Ke, Yongsheng He and Yinghuai Lu are thanked for help in the Lab. We thank Drs. J.-B, Chen, M.S. Fantle and an anonymous reviewer for constructive comments and the AE Jérôme Gaillardet for handling, which largely improved the manuscript. This work is supported by the National Natural Foundation of China (41203013, 41473017) and the fundamental research funds (2-9-2014-068) to S.A.L.

REFERENCES

Anbar A. D. (2004) Iron stable isotopes: Beyond biosignatures. *Earth Planet. Sci. Lett.* **217**, 223–236.

Balistrieri L. S., Borrok D. M., Wanty R. B. and Ridley W. I. (2008) Fractionation of Cu and Zn isotopes during adsorption onto amorphous Fe(III) oxyhydroxide: Experimental mixing of acid rock drainage and ambient river water. *Geochim. Cosmochim. Acta* **72**, 311–328.

Beard B. L. and Johnson C. M. (2004) Fe isotope variations in the modern and ancient earth and other planetary bodies. *Rev. Mineral. Geochem.* **55**, 319–357.

Beard B. L., Johnson C. M., Skulan J. L., Nealson K. H., Cox L. and Sun H. (2003a) Application of Fe isotopes to tracing the geochemical and biological cycling of Fe. *Chem. Geol.* **195**, 87–117.

Beard B. L., Johnson C. M., Von Damm K. L. and Poulson R. L. (2003b) Iron isotope constraints on Fe cycling and mass balance in oxygenated Earth oceans. *Geology* **31**, 629–632.

Bermin J., Vance D., Archer C. and Statham P. J. (2006) The determination of the isotopic composition of Cu and Zn in seawater. *Chem. Geol.* **226**, 280–297.

Bigalke M., Weyer S., Kobza J. and Wilcke W. (2010a) Stable Cu and Zn isotope ratios as tracers of sources and transport of Cu and Zn in contaminated soil. *Geochim. Cosmochim. Acta* **74**, 6801–6813.

Bigalke M., Weyer S. and Wilcke W. (2010b) Stable Copper Isotopes: A Novel Tool to Trace Copper Behavior in Hydromorphic Soils. *Soil. Sci. Soc. Am. J.* **74**, 60–73.

Bigalke M., Weyer S. and Wilcke W. (2011) Stable Cu isotope fractionation in soils during oxic weathering and podzolization. *Geochim. Cosmochim. Acta* **75**, 3119–3134.

Borrok D. M., Nimick D. A., Wanty R. B. and Ridley W. I. (2008) Isotopic variations of dissolved copper and zinc in stream waters affected by historical mining. *Geochim. Cosmochim. Acta* **72**, 329–344.

Borrok D. M., Wanty R. B., Ridley W. I., Wolf R., Lamothe P. J. and Adams M. (2007) Separation of copper, iron, and zinc from complex aqueous solutions for isotopic measurement. *Chem. Geol.* **242**, 400–414.

Brantley S., Liermann L. and Bullen T. (2001) Fractionation of Fe isotopes by soil microbes and organic acids. *Geology* **29**, 535.

Brantley S. L., Liermann L. J., Guynn R. L., Anbar A., Icopini G. A. and Barling J. (2004) Fe isotopic fractionation during mineral dissolution with and without bacteria. *Geochim. Cosmochim. Acta* **68**, 3189–3204.

Carddock P. R. and Dauphas N. (2010) Iron isotopic composition of geological reference materials and chondrites. *Geostand. Geoanal. Res.* **35**, 101–123.

Chapman J. B., Weiss D. J., Shan Y. and Lemburger M. (2009) Iron isotope fractionation during leaching of granite and basalt by hydrochloric and oxalic acids. *Geochim. Cosmochim. Acta* **73**, 1312–1324.

Dauphas N. and Rouxel O. (2006) Mass spectrometry and natural variations of iron isotopes. *Mass Spectrom. Rev.*, 25.

Dauphas N., Pourmand A. and Teng F.-Z. (2009) Routine isotopic analysis of iron by HR-MC-ICPMS: How precise and how accurate? *Chem. Geol.* **267**, 175–184.

Dauphas N., Teng F.-Z. and Arndt N. T. (2010) Magnesium and iron isotopes in 2.7 Ga Alexo komatiites: Mantle signatures, no evidence for Soret diffusion, and identification of diffusive transport in zoned olivine. *Geochim. Cosmochim. Acta* **74**, 3274–3291.

Dube A., Zbytniewski R., Kowalkowski T., Cukrowska E. and Buszewski B. (2001) Adsorption and migration of heavy metals in soil. *Pol. J. Environ. Stud.* **10**, 1–10.

Ehrlich S., Butler I., Halicz L., Rickard D., Oldroyd A. and Matthews A. (2004) Experimental study of the copper isotope fractionation between aqueous Cu(II) and covellite, CuS. *Chem. Geol.* **209**, 259–269.

Emmanuel S., Erel Y., Matthews A. and Teutsch N. (2005) A preliminary mixing model for Fe isotopes in soils. *Chem. Geol.* **222**, 23–34.

Fantle M. S. and Depaolo D. J. (2004) Iron isotopic fractionation during continental weathering. *Earth Planet. Sci. Lett.* **228**, 547–562.

Fernandez A. and Borrok D. M. (2009) Fractionation of Cu, Fe, and Zn isotopes during the oxidative weathering of sulfide-rich rocks. *Chem. Geol.* **264**, 1–12.

Gardner L. R., Kheoruenromne I. and Chen H. S. (1981) Geochemistry and mineralogy of an unusual diabase saprolite near Columbia, South Carolina. *Clays Clay Miner.* **29**, 184–190.

Huang K.-J., Teng F.-Z., Wei G.-J., Ma J.-L. and Bao Z.-Y. (2012) Adsorption- and desorption-controlled magnesium isotope fractionation during extreme weathering of basalt in Hainan Island, China. *Earth Planet. Sci. Lett.* **359–360**, 73–83.

Huh Y., Chan L. H., Zhang L. and Edmond J. M. (1998) Lithium and its isotopes in major world rivers: Implications for weathering and the oceanic budget. *Geochim. Cosmochim. Acta* **62**, 2039–2051.

Johnson C. M., Beard B. L., Roden E. E., Newman D. K. and Nealson K. H. (2004) Isotopic constraints on biogeochemical cycling of Fe. *Geochem. Non-Traditional Stable Isotopes*.

Kiczka M., Wiederhold J. G., Frommer J., Kraemer S. M., Bourdon B. and Kretzschmar R. (2010) Iron isotope fractionation during proton- and ligand-promoted dissolution of primary phyllosilicates. *Geochim. Cosmochim. Acta* **74**, 3112–3128.

Kiczka M., Wiederhold J. G., Frommer J., Voegelin A., Kraemer S. M., Bourdon B. and Kretzschmar R. (2011) Iron speciation and isotope fractionation during silicate weathering and soil formation in an alpine glacier forefield chronosequence. *Geochim. Cosmochim. Acta* **75**, 5559–5573.

Kimball B. E., Mathur R., Dohnalkova A. C., Wall A. J., Runkel R. L. and Brantley S. L. (2009) Copper isotope fractionation in acid mine drainage. *Geochim. Cosmochim. Acta* **73**, 1247–1263.

Li W., Jackson S. E., Pearson N. J., Alard O. and Chappell B. W. (2009) The Cu isotopic signature of granites from the Lachlan Fold Belt, SE Australia. *Chem. Geol.* **258**, 38–49.

Li W., Jackson S. E., Pearson N. J. and Graham S. (2010) Copper isotopic zonation in the Northparkes porphyry Cu–Au deposit. *SE Australia. Geochim. Cosmochim. Acta* **74**, 4078–4096.

Liaghati T., Preda M. and Cox M. (2004) Heavy metal distribution and controlling factors within coastal plain sediments, Bells Creek catchment, southeast Queensland, Australia. *Environ. Int.* **29**, 935–948.

Liu S.-A., Li D.-D., Li S.-G., Teng F.-Z., Ke S., He Y.-S. and Lu Y.-H. (2014) High-precision copper and iron isotope analysis of igneous rock standards by MC-ICP-MS. *J. Anal. At. Spectrom.* **29**, 122–133.

Ma J.-L., Wei G.-J., Xu Y.-G., Long W.-G. and Sun W.-D. (2007) Mobilization and re-distribution of major and trace elements during extreme weathering of basalt in Hainan Island, South China. *Geochim. Cosmochim. Acta* **71**, 3223–3237.

Ma J., Wei G., Xu Y. and Long W. (2010) Variations of Sr–Nd–Hf isotopic systematics in basalt during intensive weathering. *Chem. Geol.* **269**, 376–385.

Maréchal C. N., Télouk P. and Albarède F. (1999) Precise analysis of copper and zinc isotopic compositions by plasma-source mass spectrometry. *Chem. Geol.* **156**, 251–273.

Mathur R., Ruiz J., Titley S., Liermann L., Buss H. and Brantley S. (2005) Cu isotopic fractionation in the supergene environment with and without bacteria. *Geochim. Cosmochim. Acta* **69**, 5233–5246.

Mathur R., Titley S., Barra F., Brantley S., Wilson M., Phillips A., Munizaga F., Maksaev V., Vervoort J. and Hart G. (2009) Exploration potential of Cu isotope fractionation in porphyry copper deposits. *J. Geochem. Explor.* **102**, 1–6.

Mathur R., Jin L., Prush V., Paul J., Ebersole C., Fornadel A., Williams J. Z. and Brantley S. (2012) Cu isotopes and concentrations during weathering of black shale of the Marcellus Formation, Huntingdon County, Pennsylvania (USA). *Chem. Geol.* **304–305**, 175–184.

Millet M.-A., Baker J. A. and Payne C. E. (2012) Ultra-precise stable Fe isotope measurements by high resolution multiple-collector inductively coupled plasma mass spectrometry with a 57Fe–58Fe double spike. *Chem. Geol.* **304–305**, 18–25.

Navarrete J. U., Borrok D. M., Viveros M. and Ellzey J. T. (2011) Copper isotope fractionation during surface adsorption and intracellular incorporation by bacteria. *Geochim. Cosmochim. Acta* **75**, 784–799.

Neaman A., Chorover J. and Brantley S. L. (2005) Element mobility patterns record organic. *Geology* **33**, 117–120.

Nesbitt H. W. and Wilson R. E. (1992) Recent chemical weathering of basalts. *Am. J. Sci.* **292**, 740–777.

Nesbitt H. W. and Young G. M. (1982) Early Proterozoic climates and plate Motions inferred from major element chemistry of lutites. *Nature* **299**, 715–717.

Poitrasson F., Viers J., Martin F. and Braun J. J. (2008) Limited iron isotope variations in recent lateritic soils from Nsimi, Cameroon: Implications for the global Fe geochemical cycle. *Chem. Geol.* **253**, 54–63.

Pokrovsky O. S., Viers J., Emnova E. E., Kompantseva E. I. and Freydier R. (2008) Copper isotope fractionation during its interaction with soil and aquatic microorganisms and metal oxy(hydr)oxides: Possible structural control. *Geochim. Cosmochim. Acta* **72**, 1742–1757.

Radic A., Lacan F. and Murray J. W. (2011) Iron isotopes in the seawater of the equatorial Pacific Ocean: New constraints for the oceanic iron cycle. *Earth Planet. Sci. Lett.* **306**, 1–10.

Rubio B., Nombela M. A. and Vilas F. (2000) Geochemistry of major and trace elements in sediments of the Ria de Vigo (NW Spain): An assessment of metal pollution. *Mar. Pollut. Bull.* **40**, 968–980.

Rudnick R. L., Tomascak P. B., Njo H. B. and Gardner L. R. (2004) Extreme lithium isotopic fractionation during continental weathering revealed in saprolites from South Carolina. *Chem. Geol.* **212**, 45–57.

Ryu J.-S., Jacobson A. D., Holmden C., Lundstrom C. and Zhang Z. (2011) The major ion, $\delta^{44}/^{40}$Ca, $\delta^{44}/^{42}$Ca, and $\delta^{26}/^{24}$Mg geochemistry of granite weathering at pH=1 and T=25°C: Power-law processes and the relative reactivity of minerals. *Geochim. Cosmochim. Acta* **75**, 6004–6026.

Schoenberg R. and Von Blanckenburg F. (2005) An assessment of the accuracy of stable Fe isotope ratio measurements on samples with organic and inorganic matrices by high-resolution multicollector ICP-MS. *Int. J. Mass. Spectrom.* **242**, 257–272.

Teng F.-Z., Li W.-Y., Rudnick R. L. and Gardner L. R. (2010) Contrasting lithium and magnesium isotope fractionation during continental weathering. *Earth Planet. Sci. Lett.* **300**, 63–71.

Teng F.-Z., Dauphas N., Huang S. and Marty B. (2013) Iron isotopic systematics of oceanic basalts. *Geochim. Cosmochim. Acta* **107**, 12–26.

Thompson A., Ruiz J., Chadwick O. A., Titus M. and Chorover J. (2007) Rayleigh fractionation of iron isotopes during pedogenesis along a climate sequence of Hawaiian basalt. *Chem. Geol.* **238**, 72–83.

Tipper E. T., Galy A., Gaillardet J., Bickle M. J., Elderfield H. and Carder E. A. (2006) The magnesium isotope budget of the modern ocean: Constraints from riverine magnesium isotope ratios. *Earth Planet. Sci. Lett.* **250**, 241–253.

Vance D., Archer C., Bermin J., Perkins J., Statham P. J., Lohan M. C., Ellwood M. J. and Mills R. A. (2008) The copper isotope geochemistry of rivers and the oceans. *Earth Planet. Sci. Lett.* **274**, 204–213.

Wiederhold J. G., Teutsch N., Kraemer S. M., Halliday A. N. and Kretzschmar R. (2007) Iron isotope fractionation in oxic soils by mineral weathering and podzolization. *Geochim. Cosmochim. Acta* **71**, 5821–5833.

Wiesli R. A., Beard B. L. and Johnson C. M. (2004) Experimental determination of Fe isotope fractionation between aqueous Fe(II), siderite and "green rust" in abiotic systems. *Chem. Geol.* **211**, 343–362.

Yamaguchi K. E., Johnson C. M., Beard B. L. and Ohmoto H. (2005) Biogeochemical cycling of iron in the Archean-Paleoproterozoic Earth: Constraints from iron isotope variations in sedimentary rocks from the Kaapvaal and Pilbara Cratons. *Chem. Geol.* **218**, 135–169.

Yesavage T., Fantle M. S., Vervoort J., Mathur R., Jin L., Liermann L. J. and Brantley S. L. (2012) Fe cycling in the Shale Hills Critical Zone Observatory, Pennsylvania: An analysis of biogeochemical weathering and Fe isotope fractionation. *Geochim. Cosmochim. Acta* **99**, 18–38.

Zhu X. K., O'nions R. K., Guo Y., Belshaw N. S. and Rickard D. (2000) Determination of natural Cu-isotope variation by plasma-source mass spectrometry: Implications for use as geochemical tracers. *Chem. Geol.* **163**, 139–149.

Zhu X. K., Guo Y., Williams R. J. P., O'nions R. K., Matthews A., Belshaw N. S., Canters G. W., De Waal E. C., Weser U., Burgess B. K. and Salvato B. (2002) Mass fractionation processes of transition metal isotopes. *Earth Planet. Sci. Lett.* **200**, 47–62.

Associate editor: Jerome Gaillardet